One-dimensional models for slender axisymmetric viscous liquid bridges

F. Javier García
Departamento de Física Aplicada, E.U.I.T.A., Universidad de Sevilla, Ctra. Utrera km 1, 41013 Sevilla, Spain

Antonio Castellanos[a)]
Departamento de Electrónica y Electromagnetismo, Facultad de Física, Universidad de Sevilla, Avda. Reina Mercedes s/n, 41012 Sevilla, Spain

A set of one-dimensional models, previously derived for liquid jets, is generalized to viscous liquid bridges by applying suitably modified boundary conditions at the anchoring disks. A linear analysis for small-amplitude perturbations around the cylindrical static solution is performed. The oscillation frequencies and growth factors so obtained are compared to the already known linear three-dimensional results for a wide range in both the slenderness and viscosity. The relative error of each model is studied in terms of the typical axial length. Good agreement is found for slender enough bridges. The existence of boundary layers for weakly dissipative liquid bridges in the context of one-dimensional models is also discussed.

I. INTRODUCTION

The stability and dynamics of liquid bridges, i.e. a body of fluid anchored between two solid supports and held by capillary forces, has received much attention in the literature. The stability problem, whose solution is independent of the viscosity of the liquid, may be solved exactly using a static analysis. The solution for the linear dynamics of cylindrical inviscid liquid bridges is also well known.[1] However, its solution for viscous liquid bridges on the basis of general three-dimensional (hereafter 3-D) hydrodynamic equations involves great difficulties, and only partial results are known. Tsamopoulos *et al.*[2] have formally solved the linear problem for arbitrarily viscous liquid bridges. However, a tedious computation is necessary, and convergence is only guaranteed for Ohnesorge numbers C under 0.5. A boundary-layer treatment of this linear problem, valid for very small values of C, has been carried out by Borkar and Tsamopoulos,[3] and improved by Higuera *et al.*[4] On the other limit, Nicolás[5] has studied this linear eigenproblem for paramount viscosity.

The finite-amplitude oscillations of viscous axisymmetric liquid bridges have been studied by Chen and Tsamopoulos.[6] The nonlinear dynamic equations that describe this 3-D problem cannot be solved analytically, and hard computation is necessary in order to obtain numerical solutions.

Because of the above-mentioned difficulties, several authors have used one-dimensional (hereafter 1-D) models, initially derived for liquid jets, to study the dynamics of axisymmetric viscous liquid bridges. Most of these models[7] retain integrally the capillary pressure term. Recently, Bechtel *et al.*[8] have performed a self-consistent asymptotic 1-D analysis for slender inviscid and viscous liquid jets. Their perturbative approach develops *all* terms in the Navier–Stokes equations, including the capillary pressure one, in terms of a nondimensional wave number. The resulting leading-order models do not account for the finite instability cutoff of the exact linear 3-D analysis of Rayleigh.[9] Finite, though approximate values for this cutoff are recovered by higher-order models. This lack of accuracy is due to the truncation of the capillary pressure. In the usual 1-D models, the approach is not fully consistent from a formal mathematical point of view, in the sense that all orders in the small parameter are retained in the capillary term. However, on the one hand, it is desirable to conserve the term which leads the stability and dynamics of the physical system under consideration, and this cannot produce worse results than the Bechtel *et al.* models. As a matter of fact, the former models reproduce more accurately the well known 3-D linear results. On the other hand, the complexity of the models so derived hardly increases, and its main virtue remains unchanged: they are one-dimensional and do not depend on the radial variable.

Meseguer[10] extended the *inviscid slice model* of Lee[11] and the *Cosserat model*[12] to liquid bridges. The inviscid slice model neglects radial momentum and viscous effects. Due to its simplicity, it has been extensively used since (see Perales and Meseguer[13] for references). The correct viscous contribution has recently been derived by Eggers and Dupont[14] and, independently, by García and Castellanos.[7] In order to deal with viscous liquid bridges, some authors [10,13,15–18] have used the more elaborate Cosserat model, which enhances the Lee model in the inviscid case, since it accounts partially for radial momentum effects. Unfortunately, its range of application reduces to small viscosities, due to an inconsistency in the viscous terms.[13,7] García and Castellanos[7] have recently derived a set of 1-D models for slender liquid jets, which include the Lee, Eggers, and Cosserat models.

For slender bridges, the above-mentioned new set of 1-D models, suitably modified to take account of the boundary conditions at the anchors, is expected to be useful to find the oscillation frequencies and damping rates for arbitrary values of the viscosity. Here the results obtained with these models are compared to the linear 3-D solutions given by Sanz,[1] Higuera *et al.*,[4] Tsamopoulos *et al.*,[2] and Nicolás,[5] for invis-

[a)]Author for correspondence. Fax: 34-5-4239434, Electronic-mail: castella@cica.es

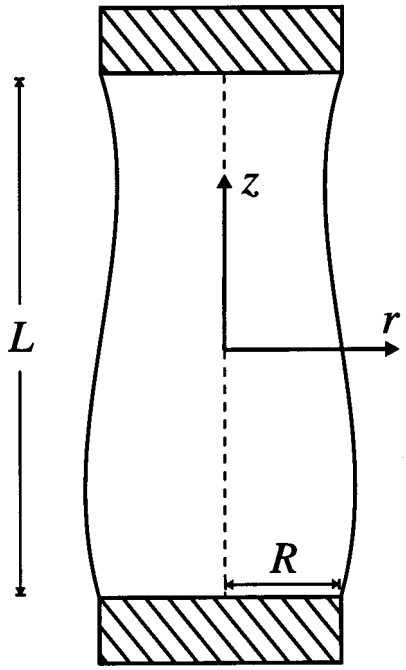

FIG. 1. Schematic description of an axisymmetric liquid bridge.

cid, weakly viscous, moderately viscous, and highly viscous liquid bridges, respectively.

In this paper, a wide range in both the slenderness ($1 \leqslant \Lambda \leqslant 10$) and the Ohnesorge number ($0 \leqslant C < \infty$) is studied, where the slenderness is the nondimensional length of the liquid bridge and the Ohnesorge number is the nondimensional viscosity (to be defined precisely below). Notice that liquid bridges of slenderness larger than π are considered. The analysis of such unstable columns is interesting for two reasons. First, it is possible to have liquid bridges of slenderness above π, using either electric[19,20] or magnetic[21] forces to stabilize the interface, or by melting a solid metal rod by means of an intense electric current passing through it.[22] Second, it is interesting to predict how many main drops, aside from the satellite drops, are going to be produced in the breaking of such slender columns, as well as to determine the minimum critical length above which these liquid bridges behave as jets.

II. EQUATIONS AND BOUNDARY CONDITIONS

Let us consider an axisymmetric liquid bridge (see Fig. 1) held between two parallel rigid circular disks of radius R, separated by a distance L, and coaxially aligned. Here the influence of the surrounding gas as well as gravity are neglected. Also density ρ, viscosity μ, and surface tension σ are supposed to be uniform and constant, and only axisymmetric configurations are considered.

The equations for the 1-D models for liquid jets are derived in detail in Ref. 7. With the latter assumptions, the same dimensionless equations apply to liquid bridges, but now additional boundary conditions at the disks must be added.

Let V and W be the radial and axial components of the velocity, which depend on r, z, and t, while the shape of the interface is given by $r = F(z,t)$. In nondimensional coordinates, the disks are placed at $z = \pm\Lambda$, where $\Lambda = L/(2R)$ is the slenderness.

Impenetrability of each of the rigid disks and anchoring to their respective edges yield

$$W(r, \pm\Lambda, t) = 0, \tag{1}$$

$$F(\pm\Lambda, t) = 1. \tag{2}$$

As long as $C \neq 0$, where $C = \mu/(\rho\sigma R)^{1/2}$ is the Ohnesorge number, the no-slip condition at the disks must be also satisfied:

$$V(r, \pm\Lambda, t) = 0. \tag{3}$$

Finally, the volume of the liquid bridge must be conserved, which gives

$$\int_{-\Lambda}^{\Lambda} dz F^2(z,t) = \int_{-\Lambda}^{\Lambda} dz F^2(z,0). \tag{4}$$

The volume of the column is important for its stability properties. However, if the dynamics of the system is under study, the conservation of volume is guaranteed by fulfillment of the continuity equation and the kinematic condition. Therefore, Eq. (4) can be considered as an initial condition.

A. Mean-velocity models

The Lee, Cosserat, and averaged models may be called *mean-velocity* models, since all of them have the mean axial velocity on a slice W and the shape of the interface F as dependent variables. Their differential order in z is four for any value of the Ohnesorge number.[7] Thus, four independent boundary conditions at the disks must be satisfied. First, the anchoring conditions (2) remain unchanged:

$$F(\pm\Lambda, t) = 1. \tag{5}$$

Second, as Meseguer[10] has shown, the radial integration of Eq. (1) on a slice implies that the mean axial velocity must be zero at the disks:

$$\overline{W}(\pm\Lambda, t) = 0. \tag{6}$$

Finally, introducing the latter four conditions in the averaged kinematic equation, which relates F to W, another two conditions for W are obtained:

$$\overline{W}_z(\pm\Lambda, t) = 0, \tag{7}$$

which are dependent with respect to (5).

It is important to note that the no-slip condition (3) leads to (7) again, as can be shown by averaging the continuity equation on a slice at $z = \pm\Lambda$. Therefore the boundary conditions at the disks are always the same, independent of the value of the Ohnesorge number.

Finally, notice that the above boundary conditions have been derived without the aid of any approximation. Thus, the relative error of the mean-velocity models, defined as the order of magnitude of the neglected terms divided by the retained ones, is expected to be the same as for liquid jets.

B. Parabolic model

The dependent variables of the parabolic model are W_0, W_2, and F. In terms of these, the velocity field is given by

$$W(r,z,t)=W_0(z,t)+\tfrac{1}{2}r^2W_2(z,t), \tag{8}$$

$$V(r,z,t)=-\tfrac{1}{2}rW_{0_z}-\tfrac{1}{8}r^3W_{2_z}. \tag{9}$$

When the viscosity is not zero, the differential order in z is eight, while it changes to six in the inviscid case.[7] This imposes the number of boundary conditions in each case.

The anchoring conditions at the edges of the rigid disks (5) apply again. If (8) and (9) are introduced in the impenetrability and no-slip conditions, (1) and (3), the following eight boundary conditions for the viscous parabolic model are obtained:

$$W_0(\pm\Lambda,t)=0, \quad W_2(\pm\Lambda,t)=0, \tag{10}$$

$$W_{0_z}(\pm\Lambda,t)=0, \quad W_{2_z}(\pm\Lambda,t)=0. \tag{11}$$

The four conditions (11) do not apply if $C=0$. Instead, substituting (8) and (9) into the kinematic equation gives another two conditions. In this particular case, the irrotationality of the velocity field allows decoupling W_2 from the problem. Therefore the following six conditions for W_0 must be fulfilled by the inviscid parabolic model:

$$W_0(\pm\Lambda,t)=0, \quad W_{0_{zz}}(\pm\Lambda,t)=0, \tag{12}$$

$$W_{0_z}(\pm\Lambda,t)-\tfrac{1}{8}W_{0_{zzz}}(\pm\Lambda,t)=0. \tag{13}$$

Conditions (13) come from imposing the anchoring of the shape of the interface to the edges of the disks. However they allow the liquid to slip on their surface, as is to be expected as long as viscosity effects are absent.

Contrarily to the mean-velocity models, the parabolic one conserves the sensitivity of the general equations and boundary conditions to the viscous or inviscid character of the problem.

III. LINEAR ANALYSIS

Let us consider small perturbations around the static cylindrical solution. The linear 1-D models previously obtained for liquid jets[7] are valid for liquid bridges, as long as the above discussed boundary conditions are added. To solve the linear dynamics associated with the 1-D models, an exponential dependence in time is tried for the variables appearing in each model:

$$f(z,t)=\mathrm{Re}[\hat{f}(z)\ \ e^{\Omega t}], \tag{14}$$

$$\overline{w}(z,t)=\mathrm{Re}[\widehat{\overline{w}}(z)\ \ e^{\Omega t}], \tag{15}$$

$$w_0(z,t)=\mathrm{Re}[\hat{w}_0(z)\ \ e^{\Omega t}], \tag{16}$$

$$w_2(z,t)=\mathrm{Re}[\hat{w}_2(z)\ \ e^{\Omega t}], \tag{17}$$

where Ω is complex in general, and its real and imaginary parts are the growth factor α and the oscillation frequency ω, respectively; and the lower case letters f, $\underline{w}$, w_0, and w_2 denote the respective perturbations of F, W, W_0, and W_2.

Although the evolution of a liquid bridge is an initial-value problem with respect to time, we do not consider initial conditions here. Instead, we address our interest to a modal analysis, from which a countable infinite set of eigenvalues Ω_m as well as their corresponding eigenfunctions are obtained. The final solution of a particular problem, characterized by its initial conditions, would be an appropriate superposition of these eigenmodes.

The above linear problem has well-defined parity with respect to z, since the equations and boundary conditions are invariant under the change of sign of z. Therefore, the eigenmodes can be classified in either antisymmetric or symmetric, according to the parity of the shape of the interface with respect to z. Note that $\overline{w}$, w_0, and w_2 have opposite parity to the shape of the interface, since applying a derivative with respect to z to any quantity changes its parity.

Similar to the dependence on time, an exponential dependence on z could be tried. However, the well-defined parity of the problem suggests proposing a combination of hyperbolic sines and cosines, which is equivalent.

A. Mean-velocity models

The substitution of the proposed dependence on both t and z in the equations of the mean-velocity models leads to the following general solution for $\widehat{\overline{w}}$:

$$\widehat{\overline{w}}=\sum_{j=1}^{2}\left[\mathscr{A}_j\cosh(\kappa_j z)+\mathscr{B}_j\sinh(\kappa_j z)\right], \tag{18}$$

where $\pm\kappa_j$ (with $j=1,2$) are the four complex roots of the biquadratic equation

$$\kappa^4+c_1\kappa^2+c_0=0. \tag{19}$$

The coefficients c_0 and c_1, which are functions of Ω, take different values for each model:
for Lee,

$$c_0=2\Omega^2, \quad c_1=1-6C\Omega; \tag{20}$$

for Cosserat,

$$c_0=\frac{2\Omega^2}{1+(C/4)\,\Omega}, \quad c_1=\frac{1-6C\Omega-\frac{1}{4}\Omega^2}{1+(C/4)\,\Omega}; \tag{21}$$

for averaged,

$$c_0=2\Omega^2, \quad c_1=1-6C\Omega-\tfrac{1}{4}\Omega^2. \tag{22}$$

Notice that the antisymmetric and symmetric modes with respect to the interface are characterized by $\mathscr{B}_j=0$ and $\mathscr{A}_j=0$, respectively.

Substitution of (18) in the linear counterparts of (6) and (7) gives two systems of homogeneous algebraic equations for the antisymmetric and symmetric modes. In order to have nontrivial solutions, the determinant formed by the coefficients of such algebraic equations must be zero. For antisymmetric modes, this yields

$$\kappa_2 \sinh(\kappa_2\Lambda)\cosh(\kappa_1\Lambda)-\kappa_1 \sinh(\kappa_1\Lambda)\cosh(\kappa_2\Lambda)=0, \tag{23}$$

while the analogous condition for symmetric modes is

$$\kappa_2 \cosh(\kappa_2\Lambda)\sinh(\kappa_1\Lambda)-\kappa_1 \cosh(\kappa_1\Lambda)\sinh(\kappa_2\Lambda)=0. \tag{24}$$

Given the parameters Λ and C, this compatibility condition is satisfied by a countable infinite set of eigenvalues Ω_m, where m is odd for antisymmetric modes and even for symmetric ones. The numerical procedure implemented to find such complex roots is described in the Appendix.

B. Parabolic model

A similar treatment can be applied to the parabolic model. The dependence on z proposed for w_0 induces an analogous one for w_2 when substituted in the equations, although with different integration constants. The resulting system of two homogeneous equations lead to the general solution

$$\hat{w}_0=\sum_{j=1}^{J}[\mathscr{A}_j \cosh(\kappa_j z)+\mathscr{B}_j \sinh(\kappa_j z)],$$
$$\hat{w}_2=\sum_{j=1}^{J}[\mathscr{A}_j\eta_j \cosh(\kappa_j z)+\mathscr{B}_j\eta_j \sinh(\kappa_j z)], \tag{25}$$

where η_j depends on C and Ω, and is given by

$$\eta_j=-\kappa_j^2\frac{\Omega-C(8+\kappa_j^2)}{2\Omega+C(16-6\kappa_j^2)}, \tag{26}$$

and $\pm\kappa_j$ (with $j=1, 2, \ldots, J$) are the $2J$ roots of

$$c_4\kappa^8+c_3\kappa^6+c_2\kappa^4+c_1\kappa^2+c_0=0, \tag{27}$$

whose coefficients are functions of C and Ω:

$$\begin{aligned} c_0&=128C\Omega^2+16\Omega^3,\\ c_1&=64C+(8-384C^2)\Omega-96C\Omega^2-4\Omega^3,\\ c_2&=48C+(7+96C^2)\Omega+18C\Omega^2,\\ c_3&=-15C-(1+14C^2)\Omega,\\ c_4&=C. \end{aligned} \tag{28}$$

Again, the antisymmetric and symmetric modes are characterized by $\mathscr{B}_j=0$ and $\mathscr{A}_j=0$, respectively.

Notice that J is the degree of the polynomial equation (27). Therefore $J=3$ if $C=0$, and $J=4$ otherwise. As shown before, the boundary conditions are also different, depending on the Ohnesorge number. Consequently, the viscous and inviscid cases must be treated separately.

If the general solution (25) is introduced in the linear counterparts of either (10) and (11) if $C\neq 0$, or (12) and (13) if $C=0$, a system of homogeneous algebraic equations for the integration constants $\mathscr{A}_j$ and $\mathscr{B}_j$ is obtained. However, a suitable combination of these equations leads to two systems of equations, one for antisymmetric modes and the other for symmetric modes.

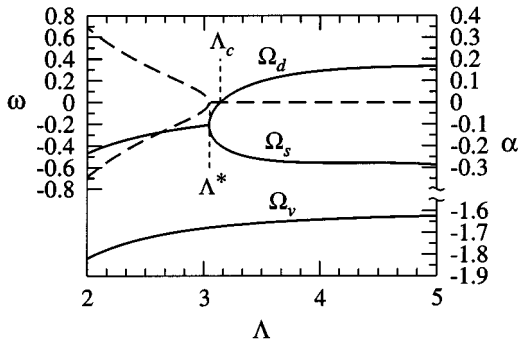

FIG. 2. Frequency ω (– – –) and growth factor α (—) versus the slenderness, as given by the parabolic model for $m=1$ and $C=0.2$.

Again, the determinants formed with the coefficients of these homogeneous systems of algebraic equations must be zero. In the viscous case, the corresponding conditions to find the antisymmetric and symmetric eigenvalues are, respectively,

$$\sum_{i,j,k,l=1}^{4}\mathscr{E}_{ijkl}\cosh(\kappa_i\Lambda)\kappa_j \sinh(\kappa_j\Lambda)\eta_k \times\cosh(\kappa_k\Lambda)\eta_l\kappa_l \sinh(\kappa_l\Lambda)=0 \quad (C\neq 0), \tag{29}$$

$$\sum_{i,j,k,l=1}^{4}\mathscr{E}_{ijkl}\sinh(\kappa_i\Lambda)\kappa_j \cosh(\kappa_j\Lambda)\eta_k \sinh(\kappa_k\Lambda) \times\eta_l\kappa_l \cosh(\kappa_l\Lambda)=0 \quad (C\neq 0), \tag{30}$$

where $\mathscr{E}$ denotes the completely antisymmetric tensor. In the inviscid case, the analogous conditions for antisymmetric and symmetric modes are

$$\sum_{j,k,l=1}^{3}\mathscr{E}_{jkl}\cosh(\kappa_j\Lambda)\kappa_k \cosh(\kappa_k\Lambda)\kappa_l(8-\kappa_l^2) \times\sinh(\kappa_l\Lambda)=0 \quad (C=0), \tag{31}$$

$$\sum_{j,k,l=1}^{3}\mathscr{E}_{jkl}\sinh(\kappa_j\Lambda)\kappa_k \sinh(\kappa_k\Lambda)\kappa_l(8-\kappa_l^2) \times\cosh(\kappa_l\Lambda)=0 \quad (C=0). \tag{32}$$

IV. RESULTS AND DISCUSSION

As will be shown below, the relative errors committed in the eigenvalues provided by the linear analysis of the 1-D models are reasonably small. In comparison with the 3-D computations, which are very heavy and present convergence problems,[2] the 1-D ones are very fast and efficient. This allows a careful parametric study of the eigenvalues and eigenfunctions, which provides valuable information about the influence of the slenderness and the viscosity on the evolution of the bridge.

Figure 2 shows the set of three eigenvalues associated with the index $m=1$, for a typical viscous liquid bridge. For each m, there is a value Λ_m^* of the slenderness under which two eigenvalues are complex conjugate, with $\alpha\leqslant 0$. For $\Lambda>\Lambda_m^*$, the latter ones become real. One of them, labeled

Ω_{dm}, increases monotonically as Λ does. The critical slenderness Λ_{cm} for which Ω_{dm} becomes positive, and therefore unstable, determines the stability of the mth mode. The other eigenvalue, Ω_{sm}, decreases monotonically. The modes corresponding to these will be called *dominant* and *subdominant*, respectively, since the former dominates the evolution of the liquid bridge, with the latter dying down relatively quickly. Thus, while nothing is said Ω_m denotes Ω_{dm}. The two modes discussed above, called *nearly inviscid* when $C \ll 1$,[4] are the only ones appearing if $C=0$. Owing to the greater differential order of the viscous equations, new modes appear as long as $C \neq 0$. These *viscous* modes have real negative eigenvalues Ω_{vm} that are approximately proportional to C for small Ohnesorge numbers, and are subdominant for realistic values of C (see Fig. 2).

The range of validity of the referred models is limited by the condition of large slenderness. Concerning the other limit, it could be thought unrealistic considering values greater than π, for which the liquid bridge is unstable. However, as we have commented before, such slender liquid columns can be obtained by applying suitable electric or magnetic fields, or by melting a solid metal rod. In particular, using electric fields,[20] dielectric liquid bridges with $\Lambda > 5$ have been obtained, and greater values of the slenderness are attainable with slight changes in the geometry of the system. If the electric field which stabilizes the dielectric liquid bridge is suddenly removed at $t=0$, the early evolution of the bridge is governed by the linear equations considered here. For $t>0$ the equations are purely hydrodynamic, because the depolarization of the liquid is instantaneous compared to any mechanical time of interest. Therefore, we will deal with slenderness within the range $1 \leqslant \Lambda \leqslant 10$. Although less realistic, much more slender liquid bridges are considered to study the asymptotic connection between liquid bridges and jets.

No restrictions have been imposed on the value of viscosity. The inviscid and very viscous cases deserve special attention, since the above-cited exact linear 3-D results provide a good test of 1-D cases in both limits. As already pointed out, the limit of small viscosity is also considered in detail, in order to compare the behavior of the 1-D models with respect to the boundary layers. Finally, we also discuss the moderately viscous case.

A. Inviscid case

In Fig. 3, the module of the most significant value of Ω_m (dominant modes) is plotted against Λ, for the first four modes and $C=0$, as calculated by Sanz.[1] The short dashed line corresponds to the growth factor of the infinite jet, taking $k=\pi/\Lambda$ as the dimensionless wavenumber, while the long dashed line is the tangent line at the maximum of the former.

Notice that, for $\Lambda \gg \Lambda_{cm}$ and $C=0$, the growth factor does not tend to zero, as happens to liquid jets. Instead it approaches a constant value which is common to all the modes, and coincides with the value of the maximum growth factor of an infinite jet. This is also true for the 1-D models for any finite value of the Ohnesorge number, and it can be explained in terms of a characteristic nondimensional axial

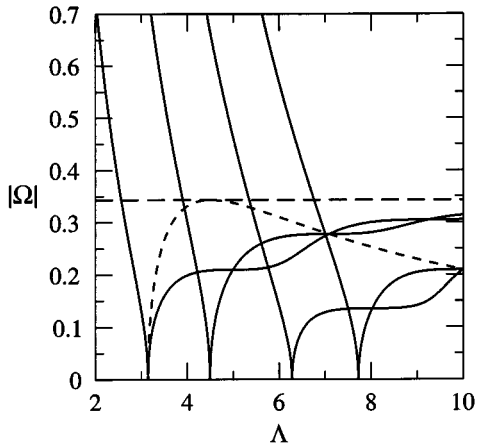

FIG. 3. Module of the eigenvalue Ω of the first four modes as a function of the slenderness, for $C=0$. The short dashed line represents the growth factor of the inviscid infinite jet. The long dashed horizontal line is the tangent at the maximum of the latter curve.

length λ, defined as the distance between consecutive nodes of the shape of the interface. λ is a half of the wavelength in a jet, but does not necessarily coincide with Λ for slender enough bridges.

Let $\lambda_{\max}$ be the value of λ for which the maximum growth factor is attained in a jet, which is about 4.51 in the inviscid case. In a bridge and for a given value of Λ, the most unstable mode should have a similar value of λ. However, this value can never be greater than Λ, which shows that the slenderness can be considered a good measure of the characteristic axial length if $\Lambda < \lambda_{\max}$ (for $m=1$). For more slender bridges, it is expected that $\lambda \simeq \lambda_{\max}$, independent of the value of Λ, and new nodes appear in the shape of the interface. In fact, this is what can be observed in Fig. 4, where the shape of the interface is plotted against z/Λ for increasing values of Λ, $C=0$, and $m=1$. For a given mode m, λ_m is approximately given by

$$\lambda_m \simeq \begin{cases} \dfrac{2\Lambda}{m+1} & \left(\text{if } \Lambda < \dfrac{m+1}{2}\lambda_{\max}\right), \\ \lambda_{\max} & \left(\text{if } \Lambda > \dfrac{m+1}{2}\lambda_{\max}\right). \end{cases} \tag{33}$$

In fact the shapes of the interface of the odd and even modes are well approximated by

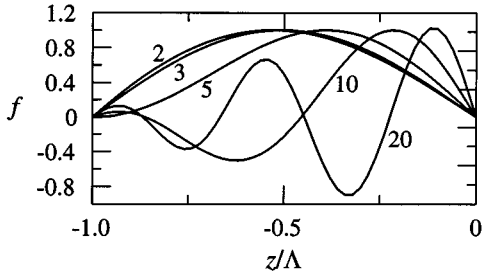

FIG. 4. Shape of the interface of the first (antisymmetric) mode versus z/Λ, for $C=0$ and $\Lambda=2, 3, 5, 10, 20$; as given by the 3-D analysis of Sanz (Ref. 1).

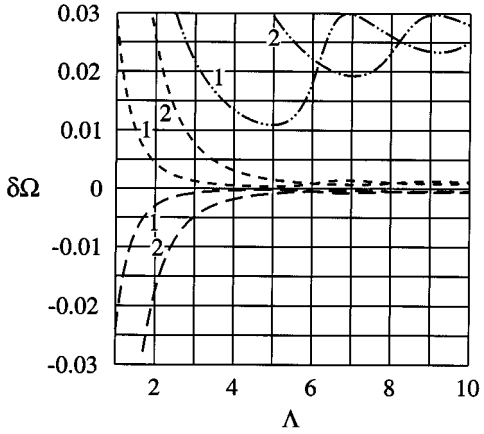

FIG. 5. Relative error in the determination of Ω by the Lee (-···-), Cosserat and averaged (– – –), and parabolic (- - -) models as a function of the slenderness, for the first two modes ($m=1,2$) and $C=0$. The numbers on the curves indicate the mode index.

$$f_{2n-1}(z)=\begin{cases}\cos\left(\dfrac{n\pi z}{2\Lambda}\right)\sin(\pi z/\lambda_{\max}) & (n=1,3,\ldots),\\ \sin\left(\dfrac{n\pi z}{2\Lambda}\right)\cos(\pi z/\lambda_{\max}) & (n=2,4,\ldots);\end{cases}\tag{34}$$

$$f_{2n}(z)=\begin{cases}\cos\left(\dfrac{n\pi z}{2\Lambda}\right)\cos(\pi z/\lambda_{\max}) & (n=1,3,\ldots),\\ \sin\left(\dfrac{n\pi z}{2\Lambda}\right)\sin(\pi z/\lambda_{\max}) & (n=2,4,\ldots);\end{cases}\tag{35}$$

where the subscript denotes the index of the corresponding mode.

The typical axial length is responsible for the relative error of the 1-D models. On the one hand, we have seen that λ is directly related to Λ if the latter is not larger than $\lambda_{\max}$. Thus, the mentioned error is expected to increase as Λ decreases or m increases, due to the decreasing distance between nodes. On the other hand, λ tends to $\lambda_{\max}$ if the bridge is slender enough. This implies that the error must tend to a constant value as Λ increases. Indeed, the above reasoning is confirmed by Fig. 5, where the data of Fig. 3 have been used to calculate the relative errors in the eigenvalue as given by the 1-D models, for $C=0$ and $m=1$ and 2.

The error of the Cosserat and averaged models, which coincide in the inviscid limit, is clearly of the same order than the one of the parabolic model. In contrast, the error of the Lee model is about twenty times greater than the previous ones. This confirms the theoretical expectations about the relative order of each of these models.

Concerning the mean axial velocity and the shape of the interface, we have found that their relative error, measured as the deviation from the exact results divided by their amplitude, is very similar to that shown above for the eigenvalues. The same is not true for the velocity components themselves, as we show below.

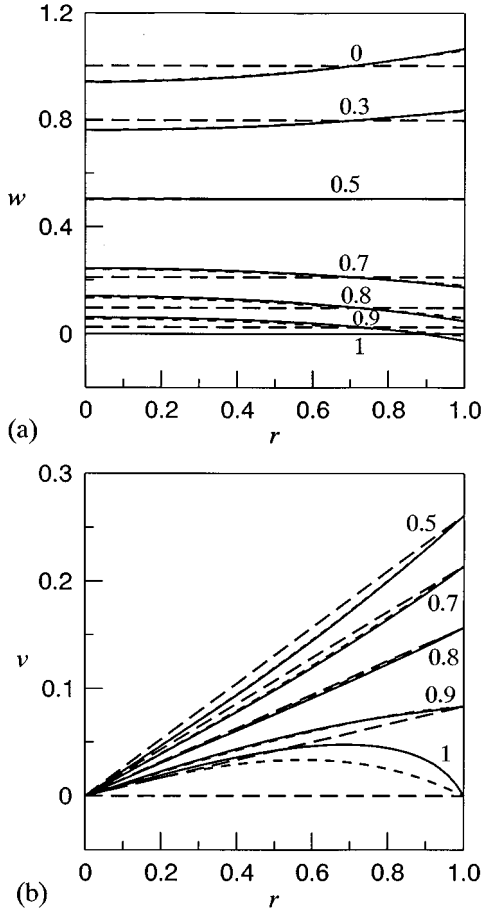

FIG. 6. Radial profile of the axial (a) and radial (b) velocities for the first mode, $C=0$, and $\Lambda=3$. The numbers indicate the values of z/Λ. Results given by Sanz (Ref. 1) (—), parabolic (- - -), and one-term averaged (– – –) approximations.

The different 1-D approximations of the velocity field can be compared to the linear 3-D solution given by Sanz[1] in the linear inviscid case. Radial profiles of the axial and radial velocities are shown in Figs. 6(a) and 6(b), respectively, for $C=0$ and $\Lambda=3$. Two approximations are plotted. On the one hand the one-term averaged one, given by Meseguer,[10] approximates W as its mean value on each slice, and V as a linear function of r. Although the averaged model has been chosen, the results are the same within the plot accuracy for any mean-velocity model, the relative error being λ^{-2}. On the other hand, the parabolic model provides a two-term polynomial approximation, whose relative error is expected to be λ^{-4}.

The one-term averaged approximation behaves worse in the center of the bridge ($z\simeq 0$) and near the disks ($z\simeq 1$). In particular, the liquid slipping on the disks is not predicted. However, it can be considered to be near the best one-term polynomial fit to the exact velocity field. In general, the parabolic approximation shows to be better than the previous one. It almost coincides with the exact results, except very near the disks, where the profile is harder to be fitted by a two-term polynomial in r. However it succeeds in describing the cited slipping on the disks, and even the slightly negative axial velocity near the anchors, already noted by Sanz.[1]

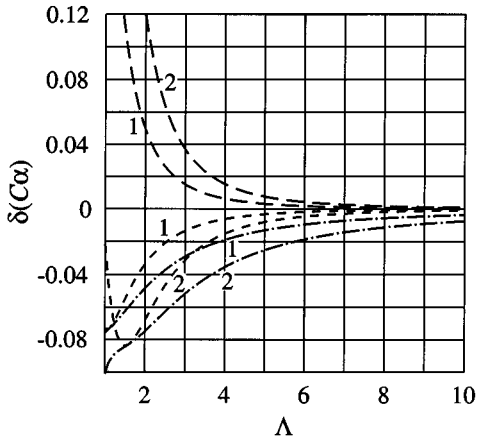

FIG. 7. Relative error in the determination of $C\alpha$ by the Lee and averaged (– – –), Cosserat (-·-), and parabolic (- - -) models as a function of the slenderness, for the first two modes ($m=1,2$) and paramount viscosity. The numbers on the curves indicate the mode index.

With respect to the role of the slenderness, the error increases as Λ decreases. The radial profiles of the axial velocity are approximately constant on a slice for slender bridges [e.g. see Fig. 6(a)]. This circumstance relaxes for smaller Λ, and the error of the 1-D approximations increases accordingly. Taking the amplitude of $\overline{w}$ as reference, the relative error in the velocity field for $C=0$ and $\Lambda=3$ is about 2% for the parabolic, and 6% for the one-term averaged approximations. For $\Lambda=2$, the analogous errors are 5% and 13%, respectively.

B. Paramount viscosity

We now focus our attention on the case when viscous effects are paramount. This holds for $C \gg \alpha\lambda^2$, which occurs not only for very large Ohnesorge numbers, but also near the stability limit.[5] Ω is real for any positive value of Λ, and its dependence on the Ohnesorge number tends asymptotically to a constant divided by C. Therefore, the quantity $C\alpha$ is considered.

The commentaries previously made about the typical axial length are valid for any value of C, provided that the wavelength of maximum growth factor for the infinite jet $\lambda_{\max}$ is computed for the given value of viscosity. This length tends to infinity as C does,[7] which means that $\lambda \sim \Lambda$ even for very slender bridges. The error must therefore tend to zero as Λ tends to infinity. This is found in Fig. 7, where the relative error of $C\alpha$ for paramount viscosity, computed through the data given by Nicolás,[5] is plotted against Λ, for $m=1$ and 2. Such deviations are related to the viscous terms neglected in the derivation of the 1-D models.

In this limit, the Cosserat model exhibits a worse agreement with the exact solution, due to the inconsistency in the second-order viscous terms. As also occurs for jets, the better results of the averaged model get worse for $\Lambda<2$, since the approximation of some viscous terms in its derivation is not very good for small slenderness. Concerning the parabolic model, the error in the first two modes does not overcome a 10% for $\Lambda \geqslant 1$. As expected, the error increases with the mode index, due to the decreasing typical axial length.

A comparison of the different approximations of the velocity field against a 3-D solution in this limit would be interesting. Unfortunately, the latter result is not available. The main features predicted by the parabolic approximation are the no slipping on the disks, and that the maximum axial velocity happens at the center of the bridge, and not at the interface as for $C=0$. This is in qualitative agreement with the 3-D results for the stream function,[5] and cannot be predicted by the one-term averaged approximation, due to its limited dependence on r.

C. Weakly viscous case

Borkar and Tsamopoulos,[3] and more recently Higuera *et al.*,[4] have studied the linear boundary-layer problem associated with weakly viscous liquid bridges. They have shown that there are two Stokes boundary layers, one at each disk, as well as another one at the interface. These regions have a very small thickness, of order $(C/\Omega_0)^{1/2}$, where Ω_0 is the eigenvalue for $C=0$. The most important correction to the inviscid values of both the damping rate and the frequency is associated with viscous dissipation at the disks (of order $C^{1/2}$), and at the bulk (of order C). The influence of the interfacial boundary layer is significantly smaller, of order $C^{3/2}$. The damping rate for small viscosities is approximately given by the real part of $\Omega_1 C^{1/2}+\Omega_2 C$. The first coefficient happens to be much smaller than the second, which justifies the second-order analysis of Higuera *et al.*[4] Consequently, the damping rate goes as $C^{1/2}$ for very small Ohnesorge numbers, while it goes as C for more realistic values of C. Due to the higher order of the viscous momentum equations, new modes appear. These viscous modes, found by Higuera *et al.*,[4] are purely damped ($\omega=0$ and $\alpha<0$), and for small viscosities their growth factor is approximately proportional to C, and only for unrealistically small Ohnesorge numbers ($C \sim 10^{-7}$ or less) do these modes become important. For increasing, not necessarily small, values of C, the damping rate of such modes also increases monotonically. Therefore the evolution of the bridge is mainly described by the most significant *nearly inviscid* modes.

The oscillation frequency and the shape of the interface are almost the same as in the inviscid case. Therefore, they are well estimated by the 1-D models. Now we examine whether these models can predict the correct values of the damping rate, the appearance of viscous modes, and the large velocity gradients present at the boundary layers. The answer is negative for the mean-velocity models and partially positive for the parabolic one, as we show below.

The damping rate, which is not zero as long as $C>0$, has been provided by Higuera *et al.*[4] In Fig. 8, the damping rate $-\alpha$ of the first mode is plotted against Λ, for $C=0.002$ and different approximations. The single crosses are data obtained numerically by Tsamopoulos *et al.*[2] Notice that, for this value of C, the result given by the parabolic model agrees very well with the data from the second-order boundary-layer analysis. The error of the mean-velocity models is clearly greater, the averaged one giving slightly worse results. This is to be expected, since the damping rate for very small C is related to the dissipation in the Stokes

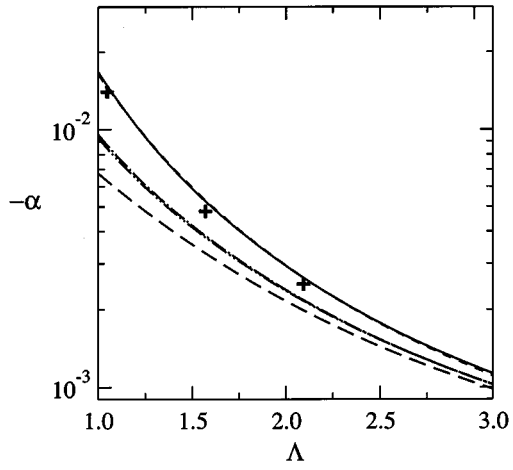

FIG. 8. Damping rate $-\alpha$ versus Λ, for the first (antisymmetric) mode and $C=0.002$. As obtained by the Lee (-···-), averaged (- - -), Cosserat (-··-), and parabolic (- - -) models; and by the boundary-layer analysis of Higuera *et al.* (Ref. 4) (—). The crosses are data from Tsamopoulos *et al.* (Ref. 2).

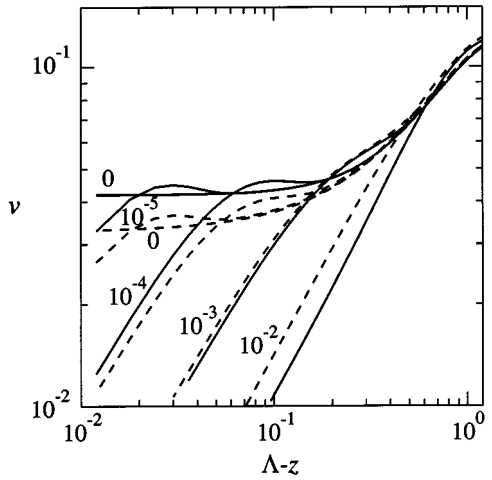

FIG. 10. Axial profile of the radial velocity near an anchoring disk, as given by the parabolic model (- - -) and the inviscid solution of Sanz (Ref. 1) as well as boundary-layer estimations obtained from the latter (—). For the first mode, $\Lambda=3$, and $r=0.5$. The numbers on the curves indicate the values of C.

boundary layers, which is not described by the latter. In general, this error diminishes as Λ increases, but is much larger than the error in the oscillation frequency.

The dependence of the damping rate on C is shown in Fig. 9, for $\Lambda=2$ and 3. Again the parabolic model is more accurate than the mean-velocity models. The dependence on C of the damping rate given by the mean-velocity models is very approximately proportional to C, which gives worse results for very small C. This seems to indicate that these models account for the dissipation in the bulk, and not for the boundary layers at the disks. As a consequence, the relative error is significantly greater in the damping rate than in the oscillation frequency. The relative error of the parabolic model also increases for very small C, but it is not proportional to C, and the error is significantly smaller.

Note also that the cited 3-D approximation differs from the 1-D ones for large enough viscosities, for which the boundary-layer analysis is not as accurate. As already pointed out, this is more evident for $\Lambda=3$, where viscous effects are greater for the same Ohnesorge number, and it becomes apparent in Fig. 8 as well.

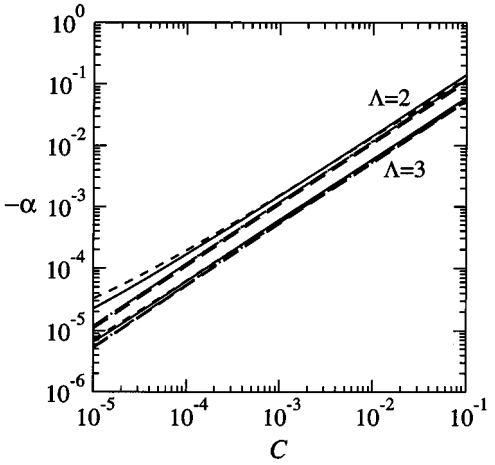

FIG. 9. Damping rate $-\alpha$ versus C, as obtained by the Lee (-···-), averaged (- - -), Cosserat (-··-), and parabolic (- - -) models; and by the boundary-layer analysis of Higuera *et al.* (Ref. 4) (—). For the first (antisymmetric) mode and $\Lambda=2,3$.

The differential order in z of the Lee, Cosserat, and averaged models is four, independent of the value of C. In addition, the boundary conditions at the disks are the same for the inviscid and viscous cases. Therefore, the mentioned mean-velocity models cannot account for the boundary layers, and no viscous modes are found. This is to be expected, since the no-slip condition on the disks does not affect either the axial velocity or its mean value. Besides, the large gradient of the axial velocity near the interface is confined to a very thin layer, whose average influence on a slice is very small. Thus, W and its derivatives change slowly as C increases from zero. The same is true for the shape of the interface, related to the former through the kinematic condition. Since the one-term approximation of the velocity field is in terms of W and F, it can only describe it in the bulk, and not in the boundary layer.

Instead, the differential order in z of the parabolic model changes from six when $C=0$ to eight when $C>0$. Besides, the number of boundary conditions at the disks changes analogously. Therefore this model accounts for the appearance of viscous modes. Although the relative error is large (up to 50% for the first two viscous modes), the importance of these modes is secondary, since they die down quite rapidly. When C is small enough, a large gradient in the radial velocity is to be expected near the wall. This is in fact found in Fig. 10, where an axial profile of the radial velocity at $r=0.5$ is plotted for several values of the Ohnesorge number, as given by the parabolic model. The 3-D inviscid solution v_0, given by Sanz,[1] is also shown. According to the leading term in the 3-D boundary-layer analysis given by Higuera *et al.*,[4] a uniform approximation to the radial velocity v can be readily found from the exact inviscid solution v_0, namely

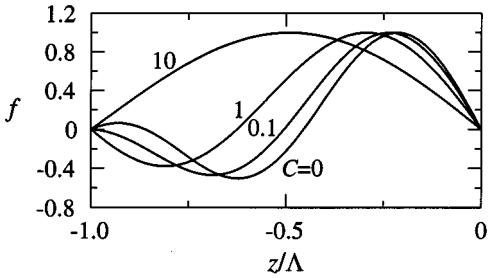

FIG. 11. Shape of the interface of the first (antisymmetric) mode versus z/Λ, for $C=0$, 0.1, 1, 10, and $\Lambda=10$, as given by the parabolic model.

$$v(r,z,t)=v_0(r,z,t)\{1-\exp[-(1+i)(\Lambda-z)/\delta]\}, \tag{36}$$

where $\delta=(2C/\omega_0)^{1/2}$ is a measure of the boundary-layer thickness, and ω_0 is the oscillation frequency for the inviscid case. This uniform approximation is also plotted in Fig. 10 for the same values of C. The gradients of the velocity field are well predicted by the parabolic model, the difference in the values of the velocity itself coming from the error of the inviscid solution.

For C greater than 10^{-2} the physical boundary layer cannot be considered narrow, and the inviscid solution does not fit the viscous one anymore. This illustrates the fact that the viscous effects may become important even for quite small values of C, provided Ω is small enough. This occurs near the stability limit for each mode, as in the preceding example, in which $\Lambda=3$.

D. Moderately viscous case

The scarce data available from a 3-D approach prevent us from doing a careful comparison. Nevertheless, some aspects related to the typical axial length, the eigenvalues, and the approximations to the velocity field are discussed.

As commented before, relation (33) holds for any given value of C, provided $\lambda_{\max}$ is computed for that Ohnesorge number. Since $\lambda_{\max}$ increases as C does,[7] the value of Λ for which new nodes appear in the shape of the interface increases. This fact is put in evidence in Fig. 11, where the shape of the interface f is plotted for the first mode, $\Lambda=10$ and several values of C, as given by the parabolic model, the other models giving similar results. Notice that the distance between nodes increases with C, and it becomes Λ for $C=10$. For the latter value of C, the viscous effects can be considered paramount.

Meseguer[10] has carried out a study of the dependence of Ω on Λ for several values of C, by means of the Cosserat model. Quite similar results are obtained with the other models derived above. A comparison to the exact linear results of Tsamopoulos *et al.*[2] is hardly interesting, since most of these are for quite thick bridges. However, relative errors can be calculated for $\Lambda=10\pi/9$ and $2\pi/3$, with $C=0.1$. For the first data ($\Lambda\simeq3.50$), the errors of the Lee, Cosserat, averaged and parabolic models are respectively 0.6%, 0.3%, 0.09%, and 0.095%; and for the second value ($\Lambda\simeq2.09$) we have 3.1%, 0.5%, 0.6%, and 0.6%. The former data show the inconsistency in the viscous terms of the Cosserat model, even for such a small value of C, and are in qualitative accordance with the corresponding results for paramount viscosities. Note that in this case the weight of the viscous terms is large, in spite of the relatively small Ohnesorge number, because $|\Omega|$ is small enough. For the first mode, this happens near its stability limit, at $\Lambda=\pi$.

V. CONCLUSIONS

A set of 1-D models, previously derived for jets, has been formulated in the field of axisymmetric viscous liquid bridges, under the hypothesis of large slenderness. The solution of the linear eigenproblem associated with each model has been compared to the available known results. It has been shown that the relative error of the cited models in determining the frequency ω and growth factor α is related to the magnitude of the typical axial length λ. For not very slender columns, $\lambda\simeq\Lambda/m$, and the index of the mode m gives the number of nodes of the shape of the interface between the disks. As Λ increases new nodes appear at the eigenfunctions, λ remains approximately constant, and the growth factor of the corresponding eigenmode tends to $\alpha_{\max}$. Since $\lambda_{\max}$ increases as C does, this explains why the cited relative errors tend to be constant for increasing values of Λ—this constant decreasing to zero as C increases from zero to infinity.

The different 1-D approximations to the velocity field have been discussed and compared in the inviscid and viscous cases. In the central region of the bridge, far from the disks, the results are similar to those for jets. The well known one-term approximation, given by Meseguer, gives an error of order λ^{-2}. An inviscid and a very viscous two-term averaged approximations, that improve the former for weakly and highly viscous liquid jets, respectively, are more accurate in the same limits of C in the central part of the bridge. However, it is worse near the disks, since they fulfill the boundary conditions for the velocity field at the disks only approximately. In contrast, the accuracy of the velocity field given by the parabolic model is satisfactory, even near the disks. It accounts for the nonzero radial velocity at the disks when $C=0$ and also predicts the large velocity gradient near the disks when C is very small.

Further work is necessary to determine the value of these models to study the breakup of liquid bridges. A common objection is that the axial length scales near the rupture might not be large, which would affect the error of these approximations.[10,18] In this sense, the work of Eggers and Dupont[14] with the viscous Lee model is very encouraging, since they predict a good agreement with a 3-D approach in the pinch region.

To conclude this study, we would like to stress the small effort necessary to find each eigenvalue and its corresponding eigenfunctions. The 1-D approach is at least four orders of magnitude more economical in time of computation than the 3-D one in the viscous case.[2] Contrarily to the latter, the former has no problems of convergence, for any value of C or Λ, and all the modes can be easily distinguished. Besides, the method of solution is formally the same for any value of the Ohnesorge number.

ACKNOWLEDGMENTS

We wish to thank to J. Antonio Nicolás and María Higuera for providing some of the data shown in Figs. 7, 8, and 9; Heliodoro González for his assistance in obtaining the data in the inviscid case; Francisco Mesa for the integral numerical method for finding zeros in the complex plane; and Antonio Ramos for helpful discussions. This work has been supported by the Spanish Dirección General Interministerial de Ciencia y Tecnología (DGICYT) under contract No. PB93-1182. F.J. García is a fellow of the Junta de Andalucía.

APPENDIX: NUMERICAL ROOT FINDING

Here we dedicate a comment to the numerical procedure employed to search out the eigenvalues Ω_m, which are the complex roots of the transcendental complex relations (23), (24), and (29)–(32).

An integral method in the complex plane has been implemented, based on the work of Mesa *et al.*[23] It gives the number of roots of a function present inside a circle in the complex plane, as well as their value. This allows an exhaustive search of zeros on the complex plane, and the desired eigenvalue can be easily followed as the control parameters of the problem change. Besides, the derivative of the function is not required. These advantages have allowed us to overcome some of the problems of differential methods like the Newton–Raphson one. The method is based on the following classical theorem, which is a consequence of the *residue theorem*:[24]

Theorem. *Let the function $g(\Omega)$ be analytic inside a region $\mathscr{R}$ of the complex plane, delimited by a closed curve Γ, such that no zeros of $g(\Omega)$ lie on Γ. If $\Omega_1, \Omega_2, \ldots, \Omega_M$ are the M zeros of $g(\Omega)$ in $\mathscr{R}$, then*

$$s_N=\frac{1}{2\pi i}\oint_\Gamma d\Omega\ \Omega^N\frac{g'(\Omega)}{g(\Omega)}=\sum_{m=1}^{M}\Omega_m^N. \tag{A1}$$

Notice that s_0 gives the number of zeros M of $g(\Omega)$ in $\mathscr{R}$. Computing $s_1, s_2, \ldots, s_M$ and applying the theorem yields an algebraic system of M equations, whose solution provides the desired roots. If the involved function has also poles at known points in the named region, it can be made regular so as to apply (A1). If there are branch points, Γ can be deformed to avoid the cuts.

In order to implement a general numerical procedure, the curve Γ is chosen to be the circle centered in Ω_0 with radius r, i.e. $\Omega=\Omega_0+re^{i\theta}$, $0\leqslant\theta<2\pi$. Furthermore, the Taylor approximation $g(\Omega)\simeq\Sigma_{k=0}^{K}b_k(\Omega-\Omega_0)^k$ is good as long as r is small enough and K is large enough. This allows us to have $g'(\Omega_0+re^{i\theta})$ in terms of $g(\Omega_0+re^{i\theta})$, by applying the Cauchy formula to obtain the coefficients b_k. The above development leads to

$$s_N\simeq\frac{1}{4\pi^2}\int_0^{2\pi}d\theta\frac{(\Omega_0+re^{i\theta})^N}{g(\Omega_0+re^{i\theta})}\sum_{k=1}^{K}ke^{ik\theta}\int_0^{2\pi}d\theta' g(\Omega_0+re^{i\theta'})\,e^{-ik\theta'}. \tag{A2}$$

The number of floating-point operations can be reduced by computing iteratively the powers appearing in the last equation. The value of K depends on the given radius r, the regularity of the function, and the number of points to do the integration. In practice, these parameters can be chosen attending to the relative error of the result, which is approximately given by s_0-M.

[1] A. Sanz, ''The influence of the outer bath in the dynamics of axisymmetric liquid bridges,'' J. Fluid Mech. **156**, 101 (1985).
[2] J. Tsamopoulos, T. Y. Chen, and A. Borkar, ''Viscous oscillations of capillary bridges,'' J. Fluid Mech. **235**, 579 (1992).
[3] A. Borkar and J. Tsamopoulos, ''Boundary-layer analysis of the dynamics of axisymmetric capillary bridges,'' Phys. Fluids A **3**, 2866 (1991).
[4] M. Higuera, J. A. Nicolás, and J. M. Vega, ''Linear oscillations of weakly dissipative axisymmetric liquid bridges,'' Phys. Fluids **6**, 438 (1994).
[5] J. A. Nicolás, ''Hydrodynamic stability of high-viscosity cylindrical liquid bridges,'' Phys. Fluids A **4**, 1620 (1992).
[6] T.-Y. Chen and J. Tsamopoulos, ''Nonlinear dynamics of capillary bridges: theory,'' J. Fluid Mech. **255**, 373 (1993).
[7] F. J. García and A. Castellanos, ''One-dimensional models for slender axisymmetric viscous liquid jets,'' Phys. Fluids **6**, 2676 (1994).
[8] S. E. Bechtel, C. D. Carlson, and M. G. Forest, ''Recovery of the Rayleigh capillary instability from slender 1-D inviscid and viscous models,'' Phys. Fluids **7**, 2956 (1995).
[9] L. Rayleigh, ''On the instability of a cylinder of viscous liquid under capillary forces,'' Philos. Mag. **34**, 145 (1892).
[10] J. Meseguer, ''The breaking of axisymmetric slender liquid bridges,'' J. Fluid Mech. **130**, 123 (1983).
[11] H. C. Lee, ''Drop formation in a liquid jet,'' IBM J. Res. Dev. **18**, 364 (1974).
[12] A. E. Green, ''On the nonlinear behavior of fluid jets,'' Int. J. Eng. Sci. **14**, 49 (1976).
[13] J. M. Perales and J. Meseguer, ''Theoretical and experimental study of the vibration of axisymmetric viscous liquid bridges,'' Phys. Fluids A **4**, 1110 (1992).
[14] J. Eggers and T. F. Dupont, ''Drop formation in a one-dimensional approximation of the Navier–Stokes equation,'' J. Fluid Mech. **262**, 205 (1994).
[15] D. Rivas and J. Meseguer, ''One-dimensional self-similar solution of the dynamics of axisymmetric slender liquid bridges,'' J. Fluid Mech. **138**, 417 (1984).
[16] J. Meseguer, A. Sanz, and J. M. Perales, ''Axisymmetric long liquid bridges stability and resonances,'' Appl. Micrograv. Tech. **2**, 186 (1990).
[17] J. Meseguer and J. M. Perales, ''A linear analysis of g-jitter effects on viscous cylindrical liquid bridges,'' Phys. Fluids A **3**, 2332 (1991).
[18] R. M. S. M. Schulkes, ''Nonlinear dynamics of liquid columns: A comparative study,'' Phys. Fluids A **5**, 2121 (1993).
[19] H. González, F. M. J. McCluskey, A. Castellanos, and A. Barrero, ''Stabilization of dielectric liquid bridges by electric fields in the absence of gravity,'' J. Fluid Mech. **206**, 545 (1989).
[20] A. Ramos, H. González, and A. Castellanos, ''Experiments on dielectric liquid bridges subjected to axial electric fields,'' Phys. Fluids **6**, 3206 (1994).
[21] A. Castellanos and H. González, ''Stability of inviscid conducting liquid columns subjected to a.c. axial magnetic fields,'' J. Fluid Mech. **265**, 245 (1994).
[22] C.-Y. Chow and M. Harvanek, ''Electromagnetic-capillary instabilities of liquid cylinder: production of spherical shells in microgravity,'' AIAA J. **28**, 372 (1990).
[23] F. Mesa, R. Marqués, and M. Horno, ''An efficient numerical spectral domain method to analyze a large class of nonreciprocal planar transmission lines,'' IEEE Trans. Microwave Theory Tech. **MTT-40**, 1630 (1992).
[24] R. A. Silverman, *Introductory Complex Analysis* (Dover, New York, 1972).